AD-A088 592 MASSACHUSETTS INST OF TECH LEXINGTON LINCOLN LAB F/G 9/5
OPTIMAL PROPERTIES OF THE CIRCULAR ARRAY FOR USE AS AN ADAPTIVE--ETC(U)
APR 80 J T MAYHAN F19628-80-C-0002
UNCLASSIFIED TN-1980-3 ESD-TR-80-27 NL

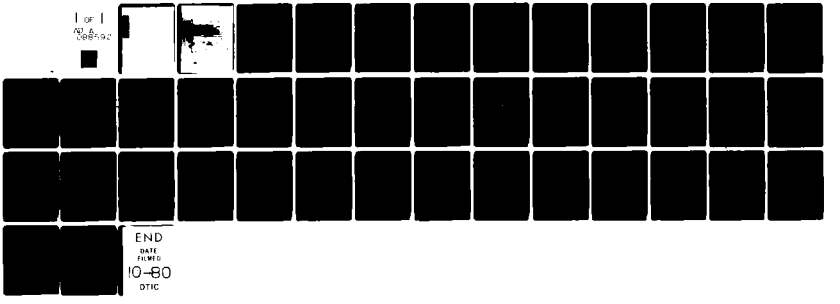

END
DATE FILMED
10-80
DTIC

MASSACHUSETTS INSTITUTE OF TECHNOLOGY
LINCOLN LABORATORY

OPTIMAL PROPERTIES OF THE CIRCULAR ARRAY FOR USE AS AN ADAPTIVE ANTENNA

J. T. MAYHAN
Group 61

TECHNICAL NOTE 1980-3

17 APRIL 1980

LEXINGTON MASSACHUSETTS

ABSTRACT

The nulling resolution of an adaptive antenna determines that spatial extent about an interference source over which the communication system's link margin is unacceptably low when the radiation pattern is shaped to place a null on interference sources present over the antenna field of view. This resolution is inversely related to D/λ, indicating that large apertures are required to achieve very narrow resolution. In order to achieve good resolution with few elements, highly thinned arrays are commonly employed. This paper develops thinned array configurations optimized in performance in accordance with specific criteria. These criteria are used to optimize the element positions within the array considering both the close-in nulling resolution, and the average coverage area over a fixed, circular field of view for which it is desired that system users have a positive link margin to a satellite at geosynchronous altitude. It is determined that the circular array configuration, with elements equi-spaced on the circle, generally produces the best close-in nulling resolution against arbitrary interference scenarios for large values of D/λ. However, the average coverage area of this array is compromised due to the high sidelobes and grating lobes generated by this configuration. Thus other array configurations are considered. It is shown that exponentially space tapering the elements on the circle improves the average coverage area with little loss in resolution, but leads to element spacings which might be incompatible with finite element size constraints in a practical design. Consequently, a third array configuration, developed according to standard synthesis techniques for non-uniform arrays, is also considered and shown to lead to good performance.

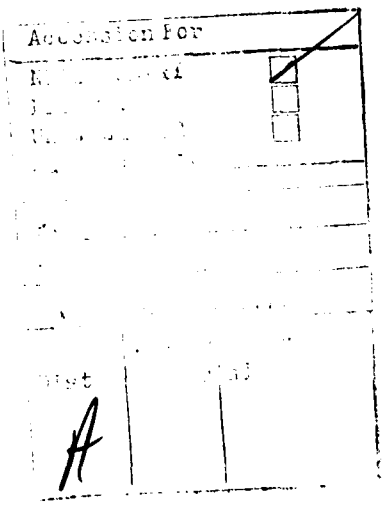

CONTENTS

ILLUSTRATIONS

Figure No.

I. INTRODUCTION

The physical limitations imposed on the angular variation of the radiation pattern realized from a finite size aperture dictate that the nulling resolution of an adaptive antenna (i.e., that spatial extent about an interference source over which the communmications system link margin is unacceptably low when the radiation pattern is shaped to place a null on the interference) is inversely proportional to D/λ where D is the aperture diameter and λ is the wavelength. Consequently, large apertures are required to achieve very narrow resolution. If the aperture is fully illuminated, then λ/D corresponds, roughly, to the half-power beamwidth (HPBW) of a maximum directivity beam formed by uniform excitation of the aperture. However, for an unfilled aperture, such as would be encountered with a highly thinned array, any number of array configurations can be specified within the given aperture diameter, each having a different HPBW. The natural question which then follows is "Which array configuration is optimum?". The answer to this question depends on many factors, not the least of which are practical constraints on the physical dimensions which might be available for housing the antenna structure, the number of elements, the directivity of each element of the array, and the interference scenario under question. It is clear that given any specific interference scenario, an array configuration can be designed to best combat the effects of the interference, although this configuration might not be optimum against a different scenario. Since communication systems must generally be designed to operate against arbitrary interference scenarios, it is necessary to tailor the antenna system against such random source locations.

The purpose of this technical note is to develop array configurations optimized in performance in accordance with specific, well-defined criteria. For simplicity, we consider the array elements to be point sources, and assume that no constraints are imposed on the placement of the elements within a given diameter. We consider planar arrays specifically, although the results are readily applicable to linear arrays with obvious modifications. The

antenna system is presumed to be operated in conjunction with an earth-geosynchronous satellite communications system serving an area on the earth defined by the angular diameter $2\theta_m$, where θ_m ($\theta_m \leq 8.7^o$) is the cone half-angle to the edge of the field of view (FOV) relative to the satellite antenna axis.

The specific criteria for optimality we use in the following analysis can be developed by considering a communications system for which a collection of users are distributed somewhat randomly over a given FOV. We assume all users require simultaneous access to the satellite, as would be the case for a frequency division multiple access (FDMA) signalling format. In the clear mode (i.e., the absence of interference), all users are served by a single element of the array, for which the element radiation pattern has a HPBW which just covers the FOV of interest. Denote this element of the array to be the "reference" element and define D_q to be the corresponding "quiescent" directive gain radiation pattern of the array with only this element excited. Define M_q to represent the "quiescent link margin" relative to thermal noise for a specific user. M_q is given by

$$M_q \equiv S_{ERP} - (S_{erp})_{MIN} \qquad (1)$$

S_{ERP} is the effective radiated power (ERP) of a specific user and $(S_{erp})_{MIN}$ is the minimum user ERP required to overcome thermal noise over the signal bandwidth in the communications receiver and all values in (1) are expressed in dB. Now consider J interference sources, each having power level $(P_j/N)_0$ relative to thermal noise at the output of the adaptive array, to be located over the FOV. The N-elements* of the array are now used to adaptively form nulls on these interference sources. After the output power resulting from

*For convenience we use the symbol N to denote both the thermal noise power and the number of elements. It is clear from the context which meaning applies.

the interference sources has been minimized, those users having quiescent margin Mq for which the uplink directive gain, D_a, satisfies the inequality

$$D_q - D_a < M_q - (I/N)_a \equiv M_e \qquad (2)$$

are still able to communicate, where $I = \Sigma P_j + N$ and $(I/N)_a$ denotes the total interference-thermal noise ratio at the receiver output after adapting to the interference scenario, and all terms in Eqn. (2) are assumed expressed in decibels (dB). Areas over the FOV for which Eqn. (2) is not satisfied are considered effectively blacked-out to the communications receiver. Note that M_e defines an effective link margin for the communications system in the presence of interference. This effective link margin determines how much loss in gain can be tolerated in the user directions over the FOV when nulls are placed on the interference sources. Ideally, adaptive processors are designed so that the interference output power is suppressed well below the thermal noise level, in which case $(I/N)_a = 0$ dB. Then M_q determines the tolerable loss in gain to the users. Practically, however, as a result of imperfections in the processor, cancellation to this level is not always possible, and M_e determines the tolerable gain loss. If M_e is small (say $\leq$ 10 dB), then placing a null on the interference sources can cause significant areas over the FOV to be blacked-out.

Two specific criteria are considered important for optimizing the design of adaptive arrays of the type described above: first, it is desired to minimize that spatial extent about each interference source which is blacked-out. This criterion is loosely referred to as the "resolution" capability of the array. To express this condition mathematically, we consider the spatial region about each interference source. Define the circular region Ω_j (solid angle), j=1, ..., J about each interference source; then, after nulls have been formed on each source in the adapted radiation pattern, the array with the best resolution about each region Ω_j maximizes the expression

$$\text{Max } R_j \equiv \max_{\substack{(x_k,\, y_k) \\ k=1,\, \ldots,\, N}} \iint_{\Omega_j} D_a \, d\Omega, \qquad j=1, \ldots, J \qquad (3)$$

where the maximization is performed over all the element coordinate positions. This condition assures that the directive gain is as high as possible in regions close-in to the interference sources.

Consider now the second condition characterizing the system performance. Clearly, the condition in Eqn. (3) places no constraint on the adapted pattern outside the regions Ω_j. Thus consideration of (3) alone could lead to good close-in resolution, but poor overall coverage area. In practice one desires to maximize the coverage area over the total FOV of interest. Otherwise said, after the array has adapted to the interference scenario, the adapted radiation pattern D_a will be significantly lower in areas close to the interference sources and also in areas where spurious minima have been generated. To incorporate this effect in our design criteria we impose the condition that the difference between D_a and D_q be minimized when averaged over the FOV, as suggested by Eqn. (2). Mathematically, this condition can be stated as

$$\text{MIN} \quad \langle |D_a - D_q| \rangle \equiv \min_{\substack{(x_k,\, y_k) \\ k=1,\, \ldots,\, N}} \iint_{\text{FOV}} |D_a - D_q| \, d\Omega \qquad (4)$$

where Ω represents the differential solid angle, the minimization is performed over the locations of the elements, and the bracket notation $\langle \cdot \rangle$ denotes the integration. Unfortunately, the minimization in Eqn. (4) is somewhat unwieldy when carried out analytically, and considerable simplification results if we place the constraint on the field patterns E_a and E_q rather than the directive gain patterns. If we define $D_a \propto |E_a|^2$ and $D_q \propto |E_q|^2$, then the condition of Eqn. (4) can be approximated by the more stringent condition

$$\text{MIN}(\varepsilon) \equiv \underset{\substack{(x_k,\, y_k) \\ k=1,\, \ldots,\, N}}{\text{MIN}} \; \langle |E_a - E_q|^2 \rangle \qquad (5)$$

where ε is defined as the RMS pattern error over the FOV. The constraint defined by (5) guarantees that the adapted radiation pattern is not unnecessarily low (so that (2) is not satisfied) in areas far from interference source positions.

Eqns. (3) and (5), when considered together, define a set of constraints which trade-off the close-in resolution against the coverage area over the total FOV. Eqn (3) can be easily evaluated analytically for single source scenarios. Rather than apply this constraint to multiple source scenarios, we will rely on computer simulations to demonstrate that the array configuration which optimizes (3) and (5) for a single source also yields good results when used against multiple source scenarios. The remainder of this paper develops as follows: *analytical solutions to Eqns.* (3) and (5) are developed in Section II, for single source scenarios, and some characteristics and properties of the solution are considered. In Section III, we examine the performance of the solutions to using Eqn. (5) as the optimum criterion for multiple interference source scenarios. Some various tradeoffs between the optimum single-source array configuation and array configurations synthesized according to other criteria (e.g., minimum grating lobes) are examined. The tradeoff between resolution, average coverage area and aperture size, for a fixed array configuration is also quantified by examining the performance of several array configurations as a function of D/λ.

II. OPTIMUM ARRAY CONFIGURATION FOR SINGLE SOURCE SCENARIOS

In this section solutions to the optimality criteria specified by Eqns. (3) and (5) will be developed and studied in detail. Since the array configuration which maximizes the close-in resolution R defined in Eqn. (3) does not necessarily yield minimum RMS error ε defined in Eqn. (5), the relative importance of each criterion must be specified. We approach this tradeoff in the following way: First we develop that array configuration which minimizes the RMS pattern error over the FOV. This maximizes the overall coverage area to users located within this area. Using this solution, we then show that the close-in resolution is determined by the location of the reference element within the aperture, and maximize R accordingly. Not surprisingly, the array configuration which minimizes the RMS pattern error over the FOV turns out to be an N-element, uniformly-spaced circular array. Furthermore, choosing a reference element located at the outer boundary of the array results in maximum resolution (as opposed to a uniform circular array with separate reference located at the array center). Physically, the optimality of the circular array configuration follows from the fact that the circular array, for equal element excitation, produces a radiation pattern which has minimum beamwidth relative to that for any other array configuration prescribed within a given circular aperture. The importance of the minimum beamwidth criterion follows by recognizing that the adapted radiation pattern, E_a, can be expressed[1,2] as a superposition of two patterns: the reference (or quiescent) pattern, E_r, and a maximum directivity (i.e., equal element weights) pattern, E_m, scanned to the location of the interference source and properly weighted so that E_r and E_m combine to form a null at this location. The resolution about the null is directly related to the beamwidth of E_m, and the choice of E_r and it follows intuitively that the narrower the beamwidth of E_m, the more rapidly the adapted pattern rises out of the null. Furthermore, the phase variation of E_r relative to E_m also influences this resolution. These results will be developed in the following paragraphs, after which we present some performance comparisons for the optimum array relative to those for other promising array configurations.

Consider the placement of N elements within a given circle. Denote normalized element coordinates (x_n, y_n), n=1, ..., N such that $x_n^2 + y_n^2 \leq 1$. The maximum directivity radiation pattern of such an array (we neglect mutual coupling effects) is given by

$$E_m(u, v) = \frac{1}{N} \sum_{n=1}^{N} e^{jux_n} e^{jvy_n} \tag{6}$$

where $u = \pi D/\lambda \sin\theta\cos\phi$, $v = \pi D/\lambda \sin\theta\sin\phi$, (θ,ϕ) are the angular coordinates (θ=0 is normal to the array) characterizing the radiation pattern and we have normalized $E_m(u,v)$ to unity at θ=0. Similarly, E_r can be expressed as a function of (u,v), denoted as $E_r(u,v)$. It follows that the adapted radiation pattern which places a null at an interference source location denoted by (u_1, v_1) or (θ_1, ϕ_1) is given by[2]

$$E_a(u,v) = E_r(u,v) - E_r(u_1,v_1)\, E_m(u-u_1, v-v_1) \tag{7}$$

Consider now the choice of the reference pattern. As discussed in Section I, for an N-element array of identical elements, the normal quiescent mode of operation uses only one element of the array. Denote the reference element location as (x_r, y_r) also assumed located within the given aperture. Since all elements are identical, the element pattern simply multiplies Eqn. (7) and can conveniently be chosen as unity without altering the results. Hence

$$E_r(u,v) = e^{jux_r} e^{juy_r} \tag{8}$$

It remains to define the regions of interest for evaluation of R and ϵ in Eqns. (3) and (5). For simplicity we consider circular regions. Define $w_0 = \pi D/\lambda \sin\theta_0$ to characterize the solid angle Ω_0 about the source location u_1, v_1 used in Eqn (3) and $w_m = \pi D/\lambda \sin\theta_m$ to characterize a circular FOV about u=0, v=0 for use in Eqn. (5). Furthermore, $E_q = E_r$ in Eqn (5). With these conditions, using Eqn. (7), the expressions for ϵ and R can be written in the form

$$\epsilon = \iint_{u^2+v^2 \le w_m^2} |E_m(u,v)|^2 \, du dv \tag{9}$$

$$R = \iint_{\Delta u^2+\Delta v^2 \le w_0^2} |E_a(u_1+\Delta u, v_1+\Delta v)|^2 \, d\Delta u d\Delta v \tag{10}$$

where Δu and Δv are incremental distances about (u_1, v_1). Since we are interested in the close-in resolution, w_0 in Eqn. (10) can be considered small, and R can be evaluated using the condition $w_0 << 1$. The integrations in (9) and (10) are tedious, but can be carried out and expressed in the forms

$$R = \frac{\pi w_0^4}{4} \left[\left(x_r - \frac{1}{N} \sum_{n=1}^{N} x_n \right)^2 + \left(y_r - \frac{1}{N} \sum_{n=1}^{N} y_n \right)^2 \right] + O(w_0^6) \tag{11}$$

$$\epsilon = \frac{\pi w_m^2}{N} \left\{ 1 + \frac{4}{N^2} \sum_{n=1}^{N-1} \sum_{m=n+1}^{N} \frac{J_1(w_m D_{n,m})}{w_m D_{n,m}} \right\} \tag{12}$$

where J_1 denotes the Bessel function of order 1, $D_{n,m}$ is the distance between the n^{th} and m^{th} element of the array and the notation $O(w_0^6)$ includes terms of order w_0^6.

Before maximizing R subject to minimum RMS error ϵ, it is interesting to note the properties of an unconstrained maximization of R. Observe that if R is maximized independently of ϵ we would obtain a rather trivial solution: that is, $x_r = -1/N\Sigma x_n$ and $y_r = -1/N\Sigma y_n$ along with $x_r^2+y_r^2 = 1$. Physically, this solution says to position the reference element along the outer boundary of the array and position the N-elements of the array at the extreme opposite of the reference element. This, in effect, yields a two-element array

geometry which generates a "line-null" across the FOV through the interference source location. Note that E_m for a two-element array has HPBW $\approx 0.5\,\lambda/D$, the smallest possible HPBW in the plane containing the two elements for any array configuration. We conclude that the two-element array yields the best achievable average resolution as defined by R, but produces a very poor pattern over the remaining FOV (furthermore, it is obvious that this array geometry cannot null more than a single interference source). Consequently, we proceed to maximize R subject first to the constraint of minimum RMS pattern error over the FOV.

Minimization of ϵ in Eqn. (12) is generally difficult for arbitrary w_m due to the highly nonlinear dependence of ϵ on the element coordinates. Consequently, we use the following approach: the small argument expansions for $J_1(x)/x$ carried out to order x^2 have the same general characteristics as the actual function for reasonably large values of x ($x \lesssim \pi$). This limiting value represents a considerably large FOV when viewed in terms of the parameter $w_m = \pi D/\lambda \sin\theta_m$. Thus our approach will be to minimize ϵ subject to the limit $w_m \lesssim \pi$ and cross-check our result against several other promising array configurations when $w_m \geq \pi$. Consider the small argument expansion $2J_1(x)/x \approx 1-x^2/8$. When used in Eqn. (12), the expression for ϵ reduces to

$$\epsilon = \pi w_m^2 \left\{ 1 - \frac{w_m^2}{4N^2} \sum_{n=1}^{N-1} \sum_{m=n+1}^{N} D_{n,m}^2 \right\} \qquad (13)$$

which is considerably simpler than (12). In fact, the expression (13) is readily maximized by noting that the array configuration which minimizes ϵ is that array configuration which maximizes the mean square distances between all the elements. It is perhaps intuitively clear that this array configuration is the circular array, with elements uniformly distributed along the outer boundary. A rigorous proof of this fact can be given, but is omitted here due to space limitations. In fact, the circular array also yields the minimum

beamwidth radiation pattern for any configuration prescribed within the aperture. It can be shown that HPBW $\approx 0.75\ \lambda/D$ for the circular array, independent of N.

Consider now the second constraint on maximum resolution. Since the uniformly spaced circular array is a symmetric array, then $\Sigma x_n=0$ and $\Sigma y_n=0$. Hence the expression for R reduces to

$$R = \frac{\pi w_0^4}{4} (x_r^2+y_r^2) + O(w_0^6) \tag{14}$$

which is clearly maximized by the choice $x_r^2+y_r^2 = 1$; i.e., choose the reference element also to be on the outer boundary. In fact, note that for all symmetric arrays, best resolution is obtained for this choice of (x_r, y_r). Physical reasons for this result are further discussed in Reference 3. Finally, we note that terms of order w_0^4 in (14) are independent of array configuration for symmetric arrays. Beyond this, terms of order w_0^6 must be used to trade-off between arrays within this sub-class. Although inclusion of these terms becomes intractable analytically, simulations will demonstrate that the circular array is consistent with maximizing R accounting for these higher order effects.

The above result is strictly valid only in the case of a single interference source. For two or more sources other factors not considered here must be accounted for. For example, it is shown in Reference 2 that nulling resolution in the presence of two interference sources is also a function of the sidelobe level of the maximum directivity pattern $E_m(u,v)$. This arises because the general form of $E_a(u,v)$ for J nulls is given by

$$E_a(u,v) = E_r(u,v) + \sum_{j=1}^{J} \alpha_j E_m(u-u_j, v-v_j) \tag{15}$$

where the α_j are adjusted so that $E_a(u_j,v_j) = 0$, $j = 1, \ldots, J$. In this case, beams $E_m(u-u_j, v-v_j)$ scanned to u_j, v_j interact with one another via their sidelobes, causing spatially connected nulls to be formed in some cases. Consequently, although more difficult to define analytically as in Eqn. (3), resolution and coverage area for $J > 1$ is dependent on the sidelobes and grating lobes of $E_m(u,v)$. Note that although it has minimum beamwidth, the circular array has very high sidelobes and many more grating lobes over a given spatial area than other array configurations. Consequently, it is interesting to consider other classes of arrays for comparison with the circular array when considering multiple interference sources. We chose three such arrays according to the following properties:

A. Tapered Circular Array

The grating lobes for a uniformly spaced circular array are positioned radially at locations $\pi D/\lambda = P \cdot N$, $P = 1,2, \ldots$, and are located at angular positions $\phi_g \approx \pi/PN$. Consequently, many such lobes exist when N is large. One way of reducing these grating lobes is to alter the uniform element spacing. Using theory developed by Ishimaru[4] and later applied by Chow[5] to space-tapered linear arrays, it was found that an exponential space tapering for the element locations of a linear array will lead to a reduced, equal-grating plateau. Such space-tapering techniques work best for large numbers of elements, and there is a limit to what can be accomplished with small values of N (say $\lesssim 20$). Nevertheless, it is interesting to consider a generalization of Chow's work applied to the circular array. Consequently, we assume that N-elements are positioned along the outer array diameter at angular locations ψ relative to the x-axis according to

$$\psi(\eta) = \pi/2 + \frac{2\pi(e^{B\eta-1})}{e^{B}-1}, \qquad 0 < \eta < 1 \qquad (16)$$

where N-elements are located according to $\eta = (n-1)/N$, $n = 1,2, \ldots, N$. Using an analysis similar to that of Ishimaru, the grating lobe positions for this space-tapering can be evaluated as a parametric function of B. It can be

shown that B $\lesssim$ 1.5 yields near optimum results for a 10-element array. For this case most of the close-in lobes relative to the uniformly spaced array move outward by a factor of 1.25, reduced in amplitude by about 3-4 dB, and the 8 dB first sidelobe of the uniform circular array is nearly eliminated. This occurs, however, at the expense of a broader main-beam. Note that the tapered circular array is a non-symmetric array.

B. Equal Area Array

Another technique used to reduce the grating plateau of regularly spaced arrays discussed by Skolnik[6] is to locate the elements according to the equal area criterion. This technique is in fact most useful for small numbers of elements. A desired aperture illumination function is chosen, and elements are located over the aperture according to positions corresponding to equal partitions of the area under the illumination function. One illumination function which works well for circular apertures (but not for linear apertures) is uniform illumination. For 10 elements the circular aperture is subdivided into 10 equal areas (one at the center and 3 angular sections having 3 elements per sector). Elements are positioned within each area according to the average location within that area; i.e., according to

$$\underline{\rho}_n = \frac{1}{A_n} \iint_{A_n} \underline{\rho}\, dS \tag{17}$$

where $\underline{\rho}$ denotes the position vector to an arbitrary point inside A_n of area dS. This positioning results in an array having one element at the center and 9 elements located outside the boundary $x_n^2+y_n^2 = 0.5$, positioned so as to produce a symmetric array. High close-in sidelobes and grating lobes are virtually eliminated using this array configuration, but the beamwidth increases by a factor of 1.3 relative to the uniform circular array.

C. Triangular Array

Finally, for comparison purposes, we consider an array having seven elements placed inside the aperture $x^2+y^2 \leq .5$, and only three outer elements. This array has an effective aperture considerably smaller than the

other arrays and thus has a much broader beamwidth, but has far-out grating lobes which are considerably reduced in amplitude. For simplicity, the elements are located according to placing one at the center, and three each on three radial arms (spaced 120^{o}) at distances of .333, .5 and 1.0 from the center.

The four types of arrays developed above are illustrated in Fig. 1. In all cases, the array is positioned such that the reference element is at $x_r = 0$, $y_r = 1$. In order to illustrate the tradeoffs between nulling resolution and array configuration, consider the following simulation. Assume the communications system is designed to operate with 10 dB quiescent link margin ($M_q = 10$). Furthermore, assume a single interference source is located over the FOV at $u = u_1$, $v = v_1$ having power level $(P_j/N)_0 >> 1$ relative to thermal noise at the receiver output. In order to model limitations which might be present in the adaptive nulling processor, assume that, after adaption, $(I/N)_a = 2$ dB, which results in cancellation of a single interference source to a level just below thermal noise. We consider only the narrowband performance of the array (more precisely we assume $\pi \cdot D/\lambda \sin\theta_m \cdot FBW << 1$, where FBW is the RF fractional bandwidth). With these assumptions, Fig. 2 illustrates, to scale, the relative areas in (u,v) space blacked-out by the interference source for each of the four array configurations. The resolution is plotted vs Δu and Δv, where $u = u_1+\Delta u$ and $v = v_1+\Delta v$. Note that the nulling resolution decomposes into two orthogonal directions. Define $\underline{\rho} = x_r\hat{x}+y_r\hat{y}$ where $\hat{x}$ and $\hat{y}$ denote unit vectors, and $\underline{\rho}_n = x_n x+y_n y$, $n=1, \ldots, N$. Furthermore, define $N\bar{\rho} = \underline{\rho}_1+ \ldots + \underline{\rho}_N$. $\bar{\rho}$ is then the average element position. Best resolution occurs along the direction $\underline{\rho}_r - \bar{\rho}$. This can be seen by rewriting Eqn. (11) for R in the form

$$R \propto \frac{\pi w_0^4}{4} \left| \underline{\rho}_r - \bar{\rho} \right|^2 \qquad (18)$$

This direction is illustrated geometrically in Fig. 2b for the asymmetric tapered circular array. Note in particular that the resolution in this plane

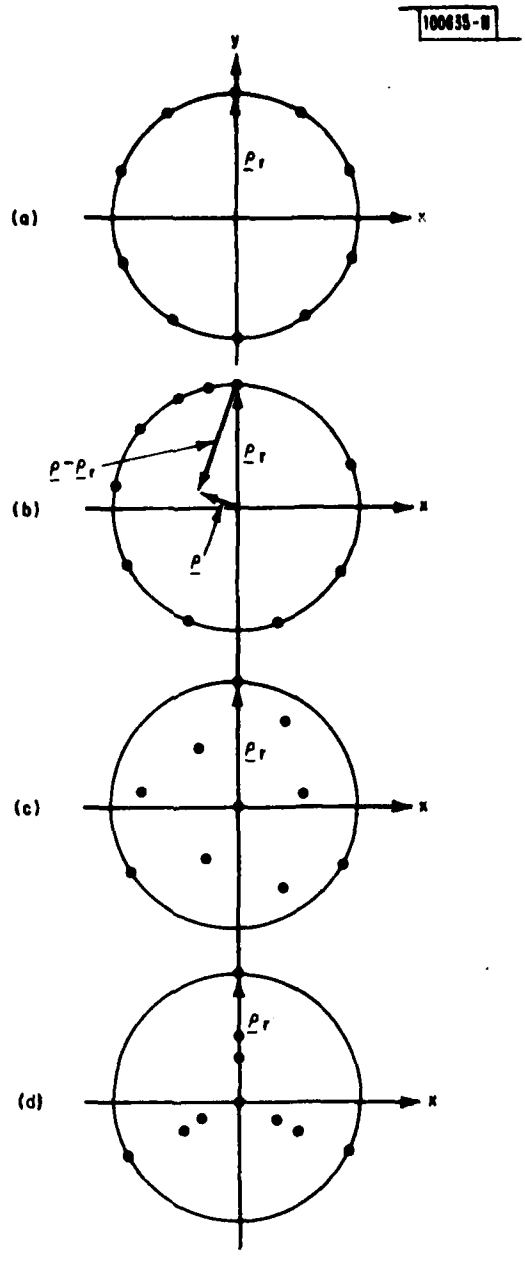

Fig. 1. Four thinned array configurations developed for comparitive performance evaluation.

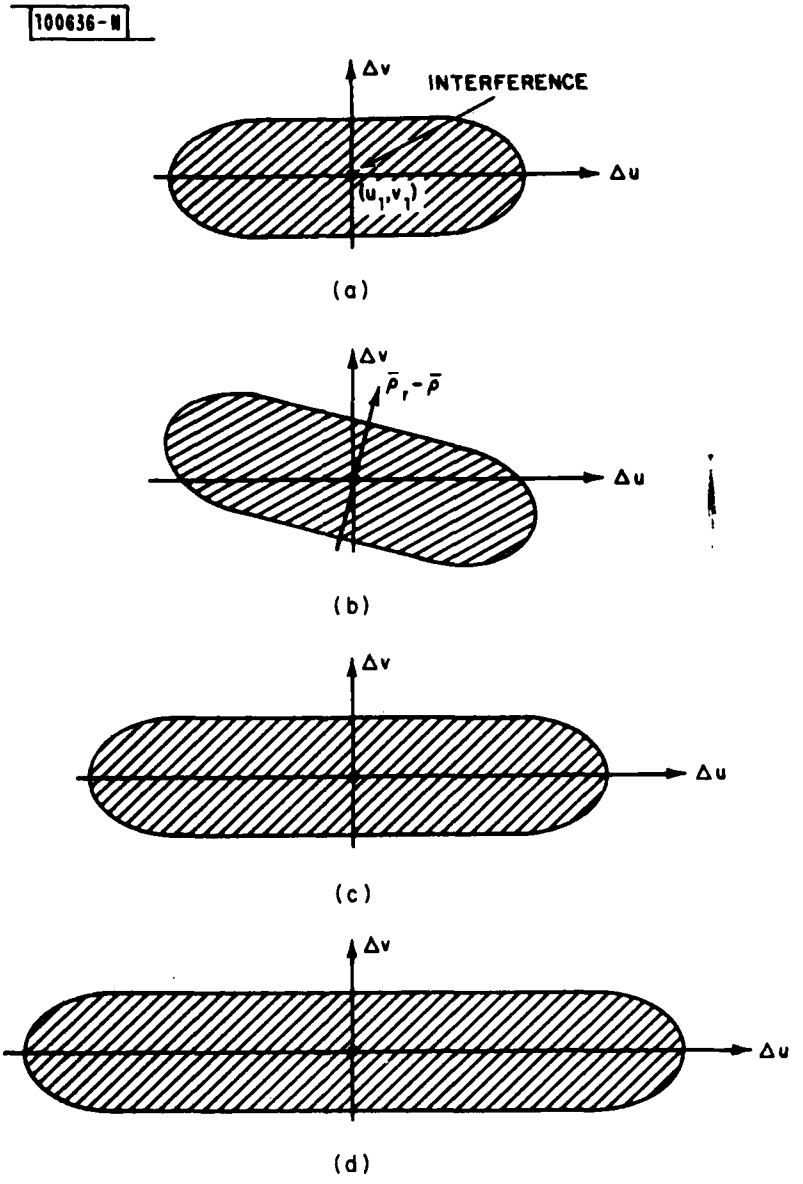

Fig. 2. Nulling resolution as a function of array configuration corresponding to the arrays of Fig. 1.

is only weakly dependent on array configuration and is dominated by the choice of reference element. For the asymmetric tapered circular array, resolution in this plane would be improved if the element used for $\underline{\rho}_r$ was chosen opposite to $\bar{\rho}$. For all the arrays, resolution is poorest in the direction orthogonal to $\underline{\rho}_r - \bar{\rho}$. In this direction, resolution is strongly dependent on the beamwidth of the maximum directivity radiation pattern $E_m(u,v)$. A simple simulation shows that the triangular array, with many elements located towards the array center, has the widest beamwidth, and the uniform circular array the narrowest. We note in passing that the overall area in the blacked out region decreases as the quiescent link margin increases, but the relative trends between configurations stay the same.

Fig. 3 illustrates the variation of the RMS error ε as a function of the parameter $w_m = \pi D/\lambda \sin\theta_m$. Recall that the small argument expansion on $J_1(x)/x$ was the dominant factor leading to the circular array as having minimum rms error. This is clearly satisfied for w_m in the range $w_m \lesssim 4.0$. However, for $w_m > 4$, the lower sidelobes and reduced grating plateau of the equal area configuration result in decreased ε when compared to the uniform circular array. For small values of w_m, ε is directly proportional to the square of the radiation pattern beamwidth, and the relative resolutions in the planes perpendicular to $\bar{\rho} - \underline{\rho}_r$ can be cross-checked with the relative values of ε for small w_m.

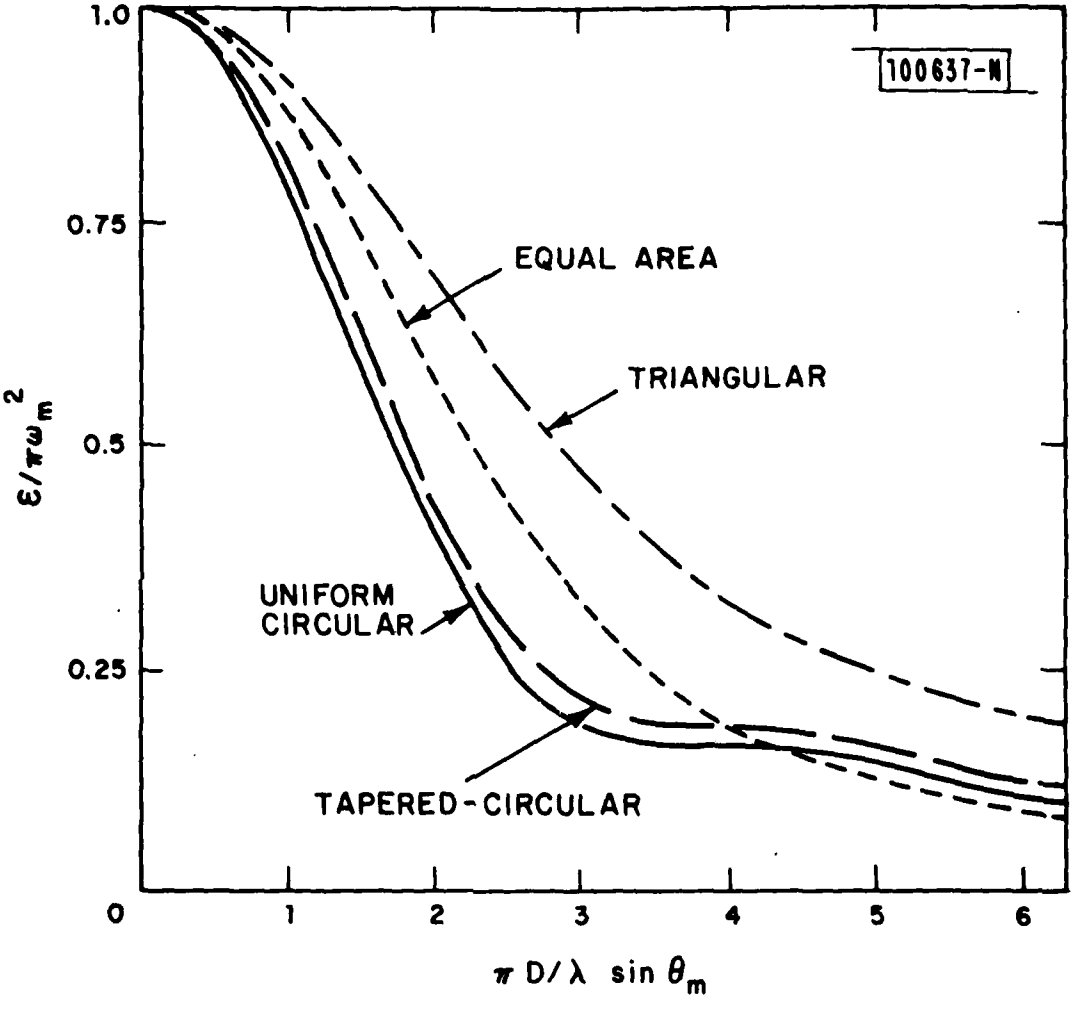

Fig. 3. RMS pattern error ε vs the parameter $\pi d/\lambda \sin\theta_m$.

III. MULTIPLE INTERFERENCE SOURCES

The results of Section II demonstrate conclusively that the uniformly-spaced circular array configuration yields optimum performance against a single, arbitrarily located interference source. In this section we will consider the performance of the uniform circular array relative to the three other baseline array configurations developed in Section II against multiple source scenarios. Recall, however, relative to the discussion pertaining to Eqn. (15), that the performance of an adaptive array against multiple interference scenarios is strongly dependent on the scenario. Consequently, it is not possible to develop a unique array configuration which performs best against all interference scenarios. However, since the precise scenario to be considered is seldom defined, it is useful to develop those array configurations whose average performance against a number of randomly generated interference source scenarios is best. Although this criterion does not lead to a unique solution, it does allow for several useful design constraints to be developed.

The performance criterion defined by Eqn. (2) is directly applicable to multiple interference scenarios. Specifically we consider that percent of the total FOV over which Eqn. (2) is satisfied relative to a specific scenario, and then average this percent coverage area over a large number of randomly generated scenarios. This average coverage area can be considered a function of several parameters: the number of interference sources, J; the quiescent link margin, M_q; the power level of each interference source, $(P_j/N)_0$; the aperture size and FOV, $D/\lambda \cdot \sin\theta_m$; and the practical constraints on the achievable cancellation limit of the processor. As in Section II, we model the processor assuming that a single source is cancelled to a level just below thermal noise at the receiver outupt; i.e., $(I/N)_a$ = 2 dB when J = 1. Furthermore, assume that multiple source scenarios contain sources of equal power level. As additional sources are added to the scenario for J > 1, then $(I/N)_a$ increases accordingly, resulting in a reduced effective link margin M_e in the presence of interference. For example, for J = 5 and M_q = 10 dB, then

M_e = 1 dB, which severely restricts the achievable resolution. We will assume the adapted weights are set according to the Applebaum-Howells type algorithm[1]

$$\underline{w} = [\underline{\underline{I}} + \mu\underline{\underline{R}}]^{-1} \cdot \underline{V} \qquad (19)$$

where $\underline{w}$ is the weight vector, R is the NxN correlation matrix defined at the antenna port outputs, and $\underline{V}$ is the steering vector given by $\underline{V}$ =[1,0,...,0] for a single element quiescent radiation pattern. The loop gain and the power level of each source is chosen such that μS_J = 32 dB when each source is transmitting seperately, where the S_k, k=1, ..., N are the N eigenvalues of R. (Therefore, the single source theoretical cancellation level would be 54 dB.) For multiple source scenarios, eigenvalues $\mu S_k < 1$ are essentially not sensed by the processor. These assumptions are consistent with practical constraints on the nulling processor limiting cancellation to approximately -30 dB for the steering vector chosen (i.e., from Reference 7, $C \leq NS_2/S_1$, where S_1 is due to the interference and S_2 is 35 dB down, limited by, say, channel tracking errors).

Before proceeding to consideration of multiple source scenarios, it is interesting to re-examine the single source results as a function of their average performance vs many scenarios, and explicitly include the dependence on the link margin M_q, and aperture size and FOV via the parameter $\pi \cdot D/\lambda \sin\theta_m$. These results are illustrated in Figs. 4, 5 and 6 for M_q = 10, 20 and 30 dB, respectively, for each of the array configurations of Fig. 1. The average percent coverage area over the circular FOV (defined by the conical half-angle θ_m) obtained using twenty randomly generated single source scenarios is plotted vs $D/\lambda \sin\theta_m$ in each figure (the results shown for J = 5 and J = 9 will be discussed below). In all cases, for any aperture size and FOV, the uniformly spaced circular array outperforms the other array configurations as predicted by the theory developed in Section II. For fixed link margin M_q, the percent coverage area approaches zero for small

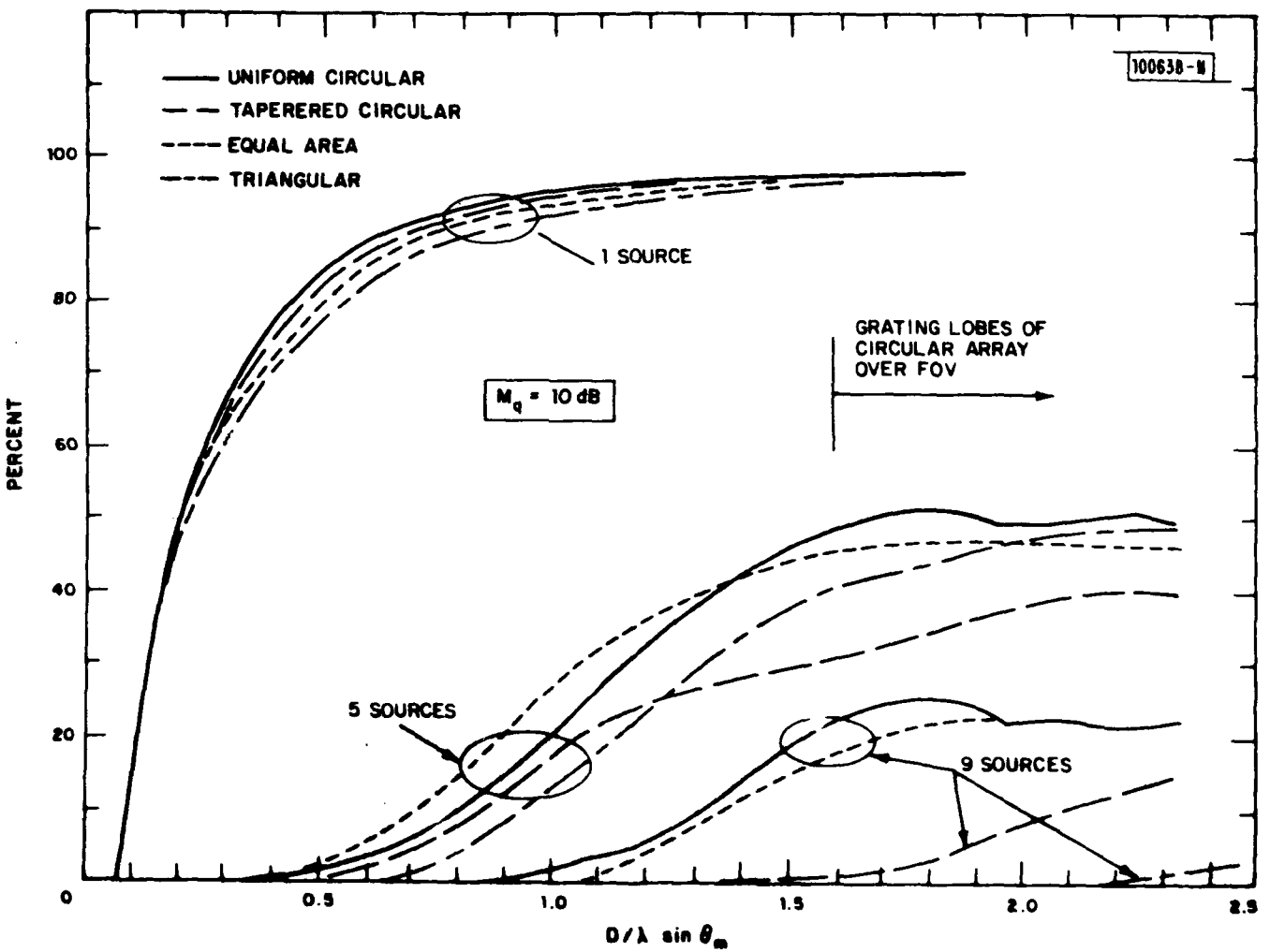

Fig. 4. Average percent area over the circular FOV having a positive link margin for M_q = 1- dB.

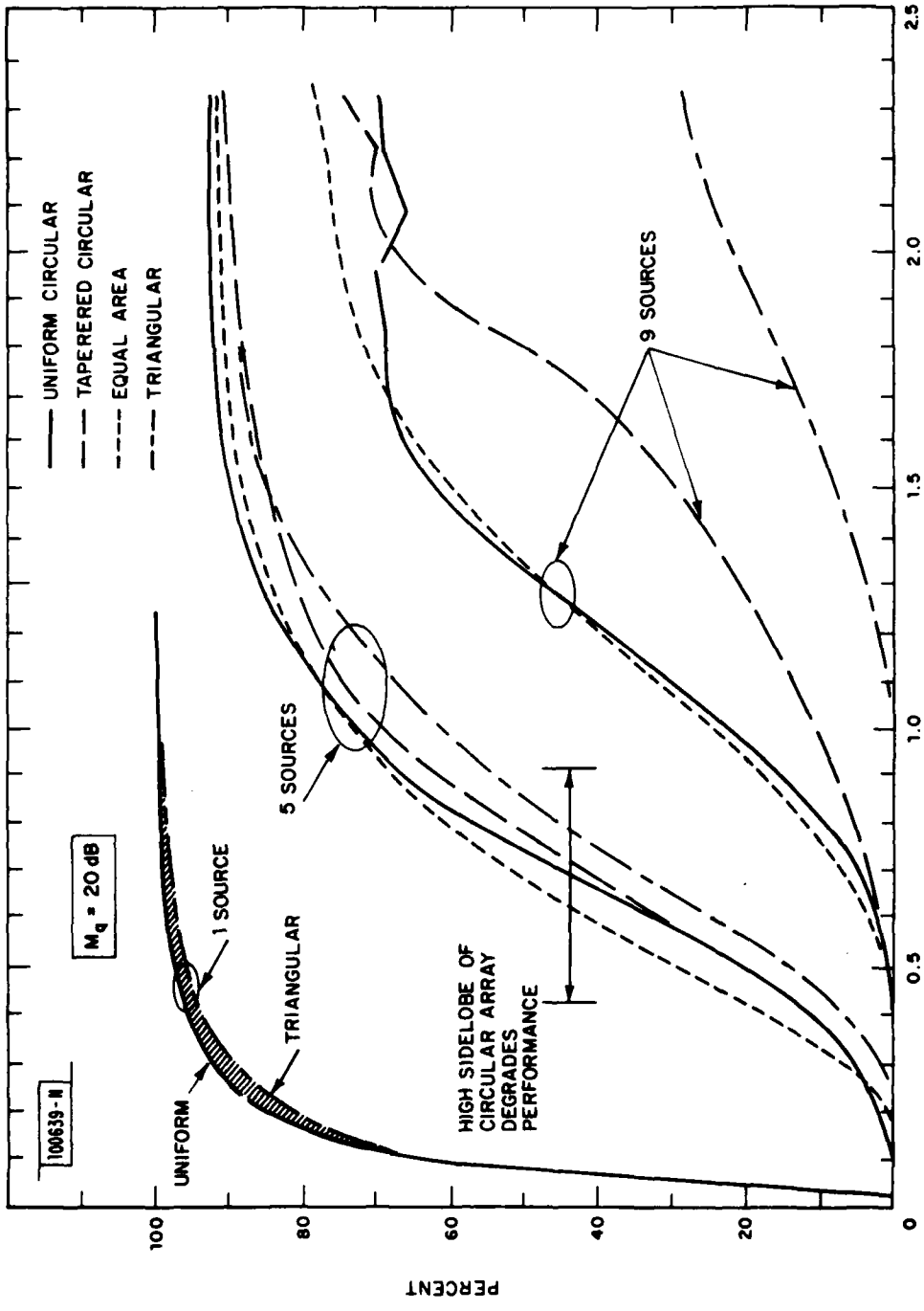

Fig. 5. Average percent area over the circular FOV having a positive link margin for M_q = 20 dB.

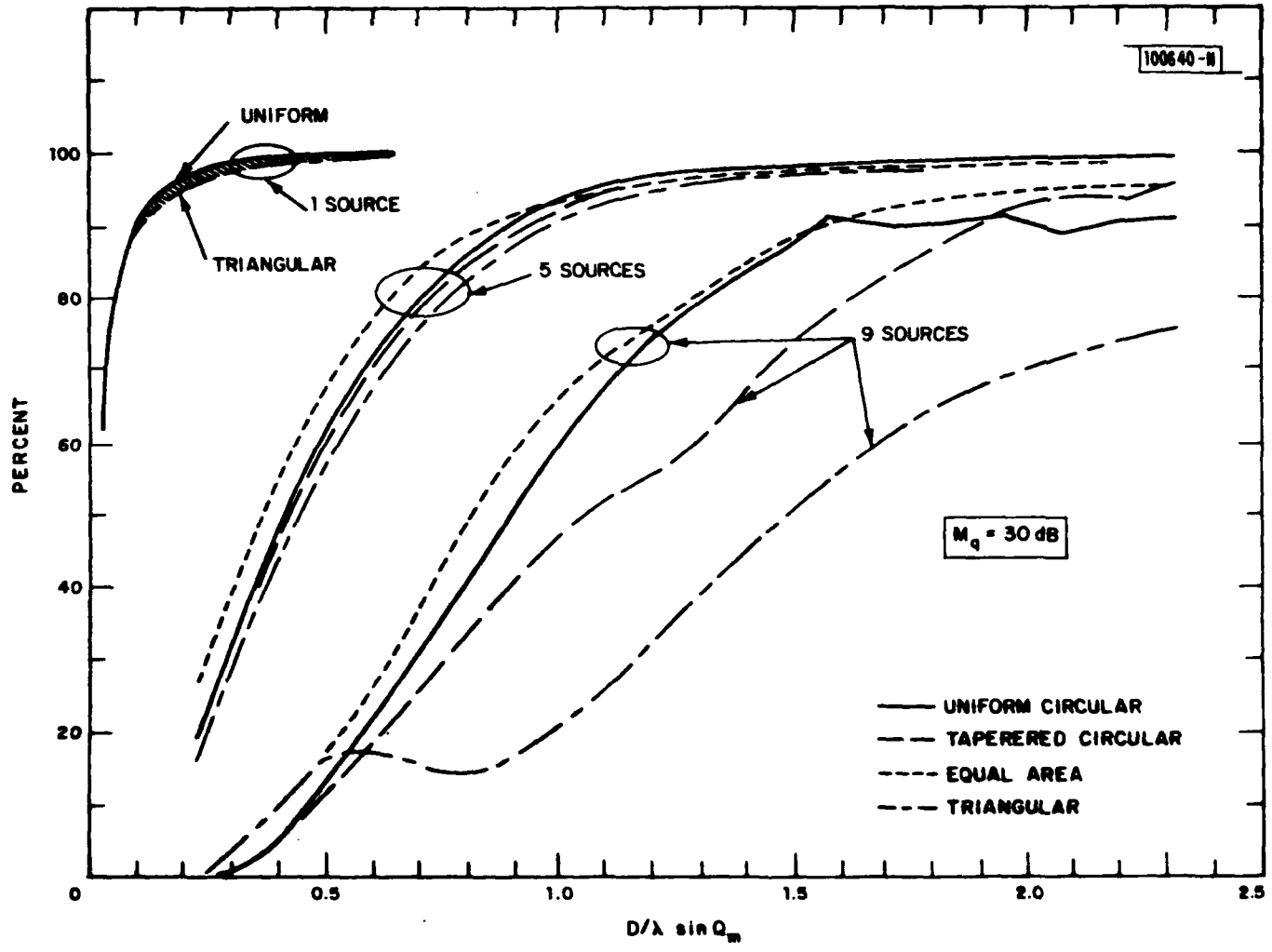

Fig. 6. Average percent area over the circular FOV having a positive link margin for M_q = 30 dB.

$D/\lambda \sin\theta_m$. This occurs because as $D/\lambda \to 0$, the null generated on the interference source encompasses the entire FOV, resulting in insufficient gain available to enable users to overcome thermal noise on the satellite receiver. The value of $D/\lambda \sin\theta_m$ where a significant fraction of the FOV becomes useable is strongly dependent on M_q. For a fixed $D/\lambda \sin\theta_m$, as M_q increases, the corresponding increase in effective link margin allows the system to operate further down on the adapted radiation pattern relative to the quiescent pattern, resulting in improved performance as M_q is increased for a given aperture size. Finally, observe that as $D/\lambda \sin\theta_m$ increases, for a given link margin, the percent coverage area approaches an upper limit less than 100% coverage area. This occurs because increasing $D/\lambda \sin\theta_m$ gives improved resolution close to the interference source, but results in a loss of coverage area away from the source due to grating nulls. This loss in coverage area just balances the gain in coverage area due to the improved resolution, leading to an average performance over the FOV independent of $D/\lambda \cdot \sin\theta_m$ for large values of this parameter. (Note that grating lobes enter the FOV when $D/\lambda \sin\theta_m \gtrsim 1.6$ for the uniform circular array.) Furthermore, observe that the improvement in resolution realized by the uniform circular array for large $D/\lambda \sin\theta_m$ relative to the other three array configurations is consistent with the resolution indicated in Fig. 2, but is difficult to ascertain from Figs. 4, 5 and 6 because the percent coverage area over the FOV for all cases is so close to 100%.

The system performance vs multiple interference scenarios follows the same general trends as for a single source, except now two factors begin to have a dominant effect: first, the practical limitations artificially imposed on cancellation achievable with the processor result in an effective link margin M_e in the presence of interference somewhat less than M_q. Consequently, the coverage area for smaller values of M_q deteriorates rapidly as J is increased. This is illustrated in Fig. 4 for M_q = 10 dB and J = 5, where at best only about 50% of the FOV has positive overall link margin for the larger values of $D/\lambda \sin\theta_m$. For a fixed M_q, as $D/\lambda \sin\theta_m$ increases, the

radiation pattern formed becomes shaped over the FOV so as to discriminate users from interference sources. Gradually a limit in average coverage area is reached for each array configuration when the increase in coverage area gained by enhanced resolution for larger values of D/λ is balanced out by the loss in coverage area due to the presence of grating nulls formed over the FOV. The limiting value of the average coverage area is dependent on M_e, which determines the tolerable gain loss in the adapted pattern.

The second major difference in system performance for $J > 1$ when compared to $J = 1$ is the effect of the near-in sidelobe and grating lobes of the uniform circular array. To see this, consider Fig. 5 which illustrates the percent coverage for $M_q = 20$ dB. Observe that for $J = 5$, the equal area array configuration outperforms the uniform circular array configuration over a wide range of values when $D/\lambda \sin\theta_m$ is small. This occurs because, for smaller D/λ, only the main beam and near-in sidelobes of $E_m(u-u_j, v-v_j)$ exist over the FOV. Refering to Eqn. (15), we note the effect of the interaction of $E_m(u-u_j, v-v_j)$ and $E_m(u-u_i, v-v_i)$, where "j" and "i" correspond to different interference source locations, occurs via the near-in sidelobes. Thus although the circular array has minimum beamwidth, it has a very high 8 dB sidelobe close-in to the main beam, resulting in "connected" nulls being formed between sources for some scenarios. These result in a decrease in overall coverage area. To demonstrate this tradeoff, Fig. 7 illustrates radiation pattern cuts in the $v = 0$ plane of $E_m(u,v)$ for both the uniform circular array and the equal area array. Observe that for $u > 2.94$, the equal area array actually has lower pattern values, which leads to minimum interaction between adjacent interference sources. Note, however, that as D/λ increases for a fixed scenario and FOV, sources appear further apart relative to HPBW for each array, so that this interaction gradually disappears. After this point the narrow beamwidth of the circular array results in better performance for this array. Since the overall array diameter would generally be chosen so as to operate beyond the "knee" of the percent area curve, in order to maximize the percent coverage, the circular array still yields

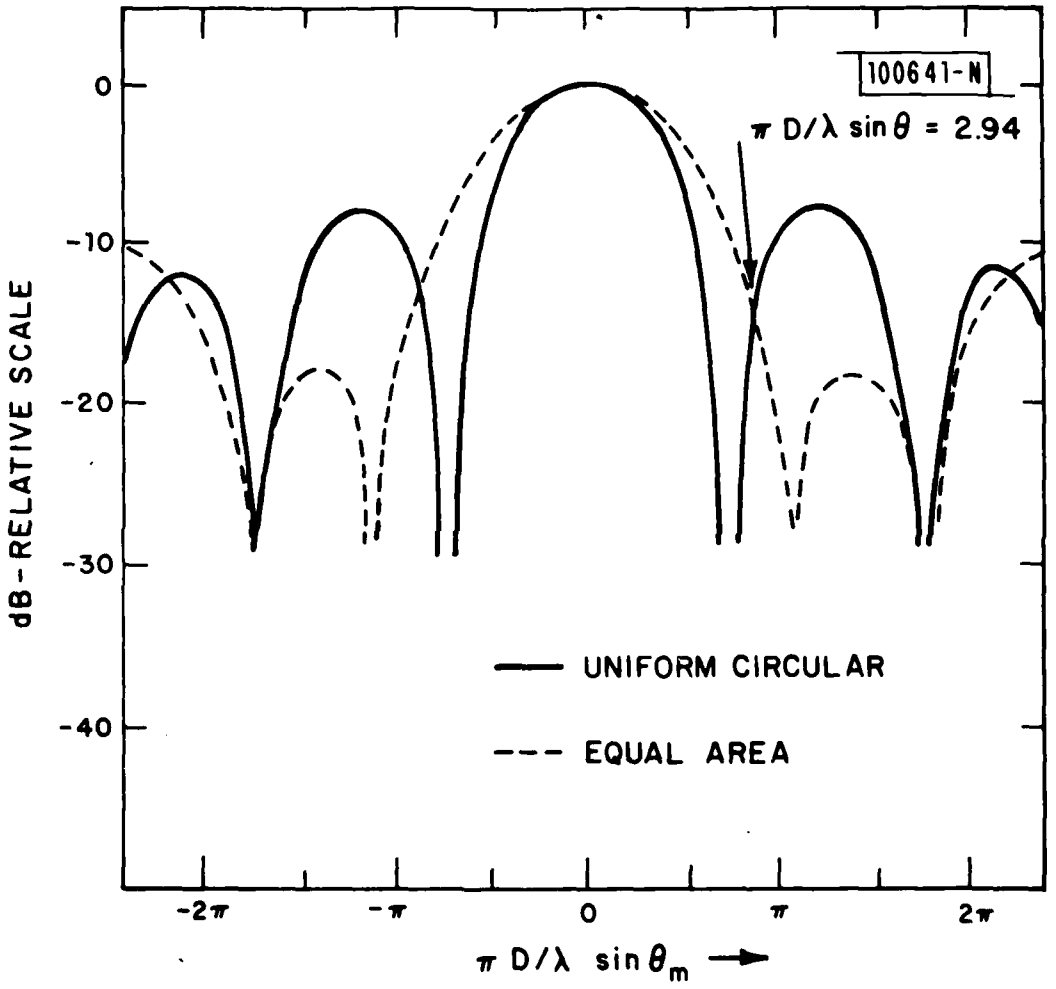

Fig. 7. Radiation pattern cuts in v=0 plane of $E_m(u,v)$ for the uniform circular array and the equal-area array.

optimum performance relative to the other arrays when considered in a design tradeoff study. Of course, for very large D/λ, the circular array always yields the best close-in resolution because of the minimum beamwidth of $E_m(u,v)$, but the presence of numerous grating lobes for this array limits its overall performance when averaged over the total FOV to just slightly better than the other arrays. In this respect, the advantages of tapering the elements along the outer circle should be considered, as this reduces the grating lobes considerably. The improvement realized in this case is most dramatic as the number of sources increases, as will become obvious from the results below for $J = 9$ for the tapered circular array. Finally, note that the poorer performance of the triangular array for smaller values of D/λ is directly related to the corresponding broader beamwidth of $E_m(u,v)$ for this array when compared to the others.

The performance for $J = 9$ in Figs. 4, 5 and 6 is unique in that nine sources correspond, for the 10 element array, to N-1 sources being nulled by an N-element array. This, in fact, provides maximum stress on the array's ability to minimize the total output power. First observe in Fig. 4 that, for all the array configurations, the performance for $J = 9$ and $M_q = 10$ dB is dominated by the negative effective link margin $M_e \approx 0$ dB (i.e., $(I/N)_a \approx 10$ dB for $J = 9$). In this case only values for D_a which peak up greater than D_q provide position overall link margin to the satellite. This emphasizes the need for a sizeable quiescent margin for systems where processor imperfections limit the achievable cancellation.

Consider the results of Fig. 6 for $M_q = 30$ dB, for which sufficient quiescent margin exists to achieve greater than 90% coverage area when $J \geq 5$ and the larger values of $D/\lambda\sin\theta_m$. This situation would be indicative of system performance for which there are no limitations on the cancellation achievable by the processor, and $M_q >> 1$. It is for this case that the most striking differences in performance between the 4 array configurations occur. Note that for very small D/λ, the triangular array gives near optimum performance, albeit a very small coverage area when $J = 9$. This is due

entirely to the resolution realizable from the three outer elements of this array. For small D/λ, these three elements are sufficient to collectively null nine sources which might be positioned together over one area of the FOV. (Recall, the results of Figs. 4, 5 and 6 characterize the average performance. For some scenarios, the entire FOV is blacked-out out for these smaller values of $D/\lambda\sin\theta_m$.) However, as $D/\lambda\sin\theta_m$ increases, the inner elements of the array must be used and eventually the point is reached where the array has much less effective aperture, as is evident from the results shown in the figure. This leads to considerably poorer performance for the triangular array relative to those arrays where the elements are located toward the outer edge of the aperture.

The general trends for the remaining arrays for $J = 9$ and $M_q = 30$ dB are more or less the same as for $J = 5$. Note, however, that the grating nulls of the uniform circular array dominate its performance sufficiently enough so that poorer overall performance relative to the average coverage area is realized for this array relative to the equal area and tapered-circular arrays. Note also that for larger D/λ, the performance of the tapered circular array begins to improve considerably as a consequence of the grating lobe reduction of $E_m(u,v)$ achieved via the exponential spacing for space tapering the array.

In order to obtain more of a physical feel for the above results, it is useful to examine the link margin contours for each of the arrays for a typical random scenario used in obtaining the results of Fig. 6. Consider the case $M_q = 20$ dB, $\pi D/\lambda\sin\theta_m = 6.6$ and a sample 9-source scenario. The area over the FOV blacked-out to system users for this case is illustrated in Figs. 8, 9, 10 and 11 for each of the array configurations of Fig. 1, respectively. The general trends discussed above are evident. The uniform circular array configuration offers good resolution, but the average coverage area deteriorates due to spatially connected nulls between sources resulting from the high sidelobes and grating lobes of $E_m(u,v)$ for this configuration. Exponentially tapering the elements yields the results of Fig. 8. Note that

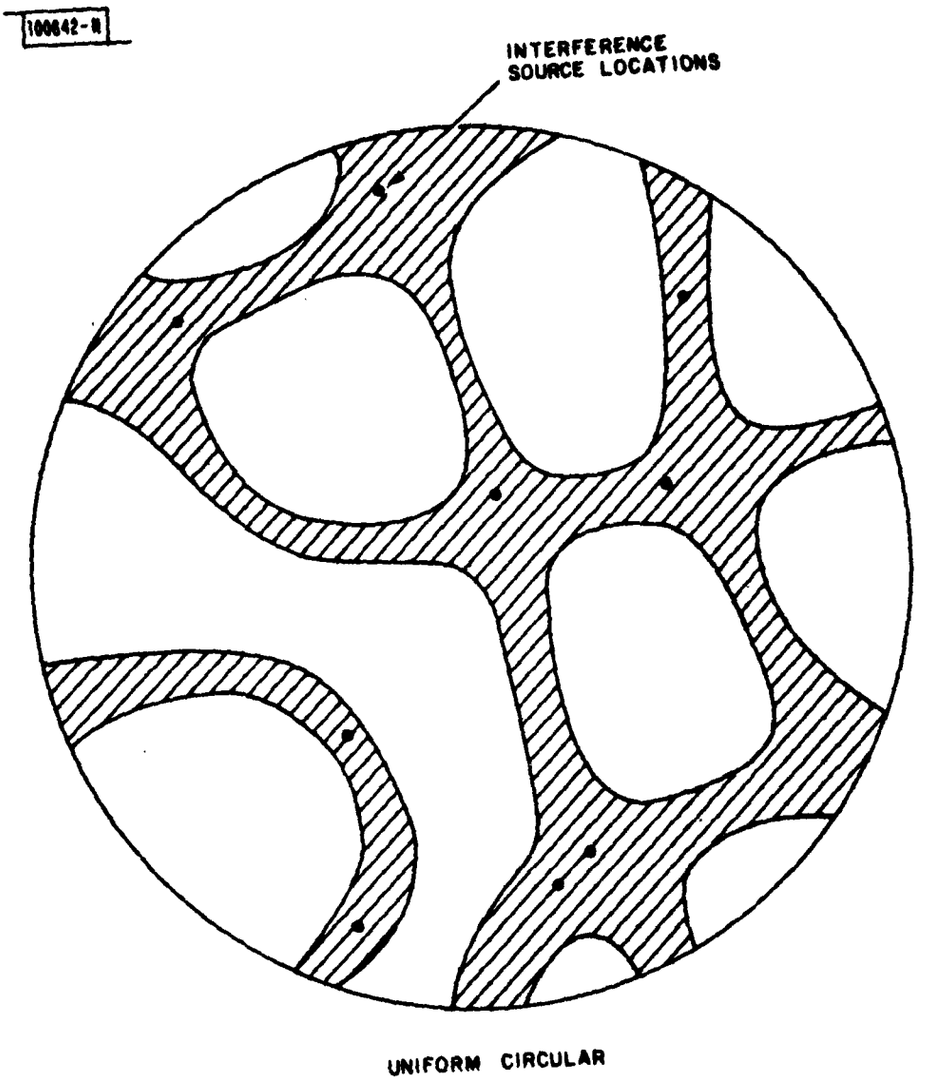

Fig. 8. Coverage for a sample 9-source scenario using the uniform circular array. M_q = 20 dB.

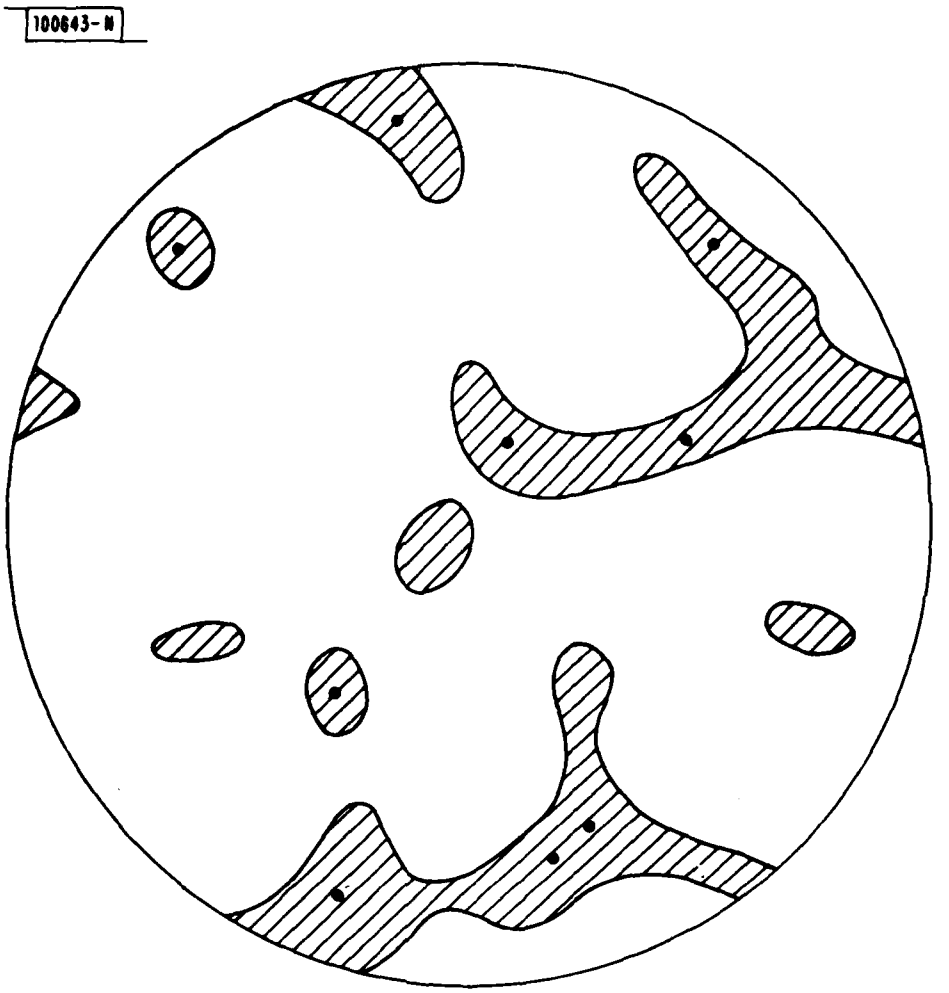

Fig. 9. Coverage area for a sample 9-source scenario using the tapered circular array. M_q = 20 dB

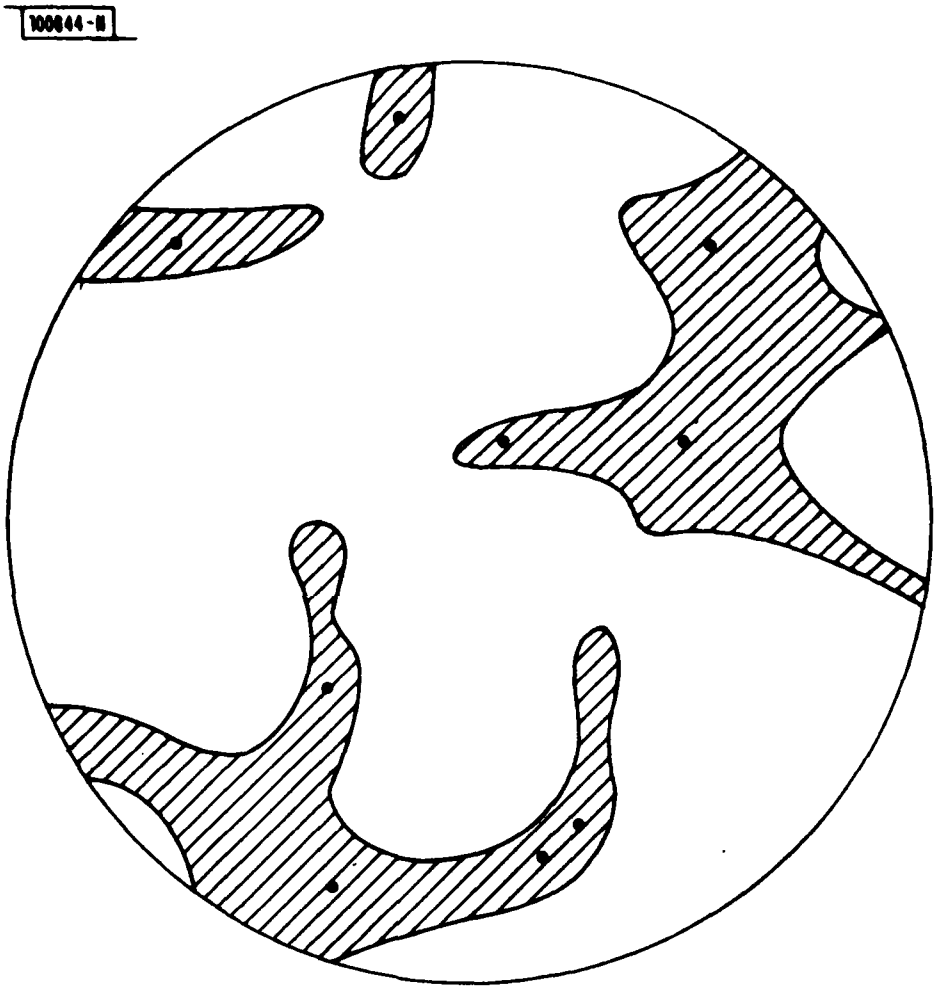

Fig. 10. Coverage area for a sample 9-source scenario using the equal-area array. M_q = 20 dB

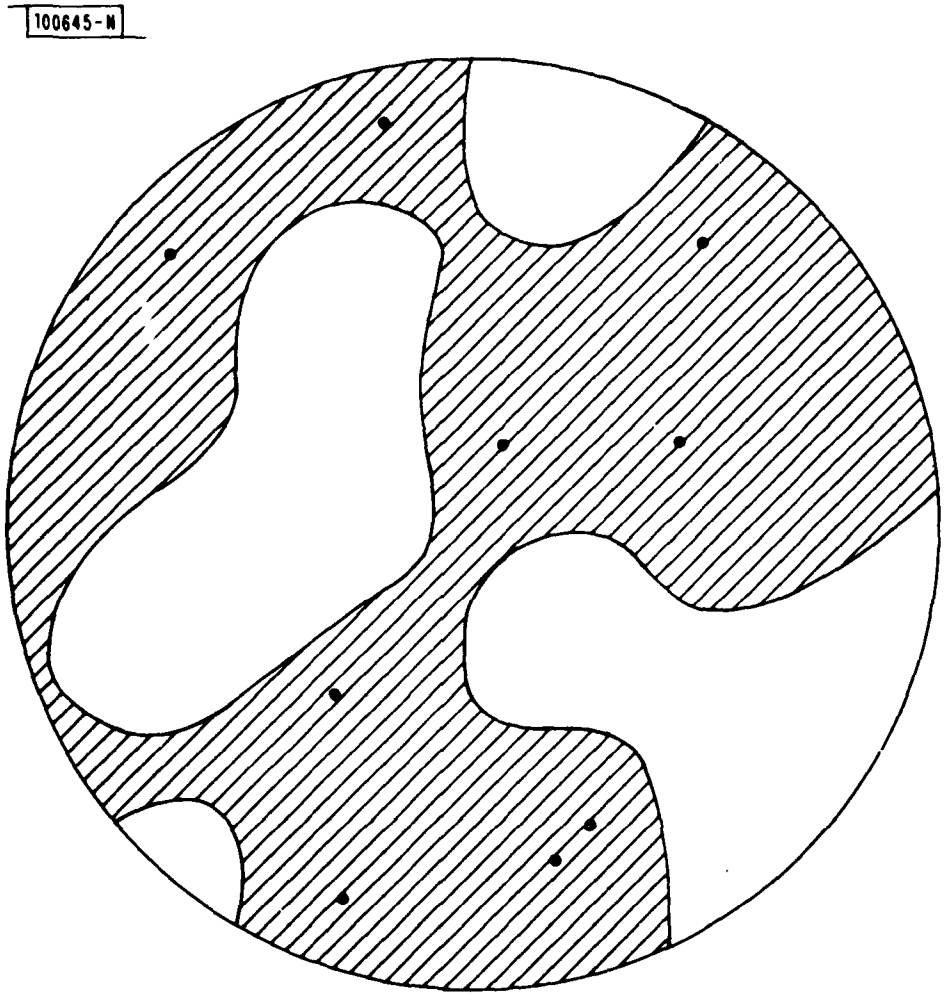

Fig. 11. Coverage area for a sample 9-source scenario using the triangular array. M_q = 20 dB

the close-in resolution is preserved, and the average coverage area has increased. The results for the equal-area array also yield good average coverage area, but the close-in resolution has been compromised somewhat. Finally, it is clear from the results of Fig. 10 that the poor coverage area for the triangular array is due to the locations of the seven innner elements inside $\rho_n \leq .5$, leading to much less effective aperture.

IV. SUMMARY

We have considered the problem of developing array configurations optimized in performance relative to an earth-geosynchronous satellite communications system designed for use with adaptive antenna nulling on the uplink. Two complementary optimality criteria have been developed for evaluation of the array performance: maximum percent coverage area to a set of users located over a given FOV, when averaged over a large number of interference source scenarios; and maximum nulling resolution about a given interference source (as defined by Eqn. (3)). With these goals in mind, it was determined that the circular array configuration having elements equi-spaced on the circle produces the minimum beamwidth, maximum directivity radiation pattern $E_m(u,v)$ as defined by Eqn. (6). Since the radiation pattern formed by any adaptive array configuration is characterized by linear combinations of such maximum directivity beams (see Eqn. (15)), the circular array configuration generally produces the best close-in nulling resolution against any interference scenario as the parameter $D/\lambda \sin\theta_m$ increases indefinitely. However, this enhanced close-in spatial resolution is not always consistent with the constraint of maximum coverage area over the overall FOV because of the enhanced grating lobes properties of $E_m(u,v)$ for such a uniform array. Consequently, the performance of this array was evaluated relative to arrays space-tapered so as to reduce the grating lobes of $E_m(u,v)$. It was found that exponentially space-tapering the elements along the outer circle leads to significant improvement for large values of D/λ. However, this leads to some elements in close proximity to one another, which may not be compatible with the finite element size required in an actual array design. Thus alternate array configurations were considered. A third array configuration, generated using the non-uniform array synthesis technique discussed by Skolnik[6], was found to realize a performance close to, and in some cases, superior to, the uniform and tapered circular arrays. For this configuration elements are located so as to correspond to equal areas over a circular aperture. All elements except the center one lie outside the circle

$\rho = 0.5$, where ρ is the distance from the center of the aperture. This array yields a pattern $E_m(u,v)$ with reduced grating lobes and lower near-in sidelobe when compared to those for the uniform and tapered circular arrays. However, the broader beamwidth leads to reduced close-in resolution for single source scenarios, but better performance against multiple source scenarios for intermediate values of the parameter $\pi \cdot D/\lambda \cdot \sin\theta_m$.

For situations where physical considerations on aperture size, element size and inter-element spacing constrain one from using the uniform circular array geometry, several design guidelines can be enumerated for choosing the near-optimum array configuration: First, position the elements radially outward as far as possible over the aperture. Secondly, if a single element reference (or quiescent) radiation pattern is to be used, choose an element on the outer boundary as the reference. Lastly, choose the overall diameter of the array consistent with the desired resolution for users located close-in to the interference source. The resultant array configuration will then necessarily yield near-optimum performance when averaged over the total FOV. These results apply strictly to narrowband nulling, i.e., cases where $\pi D/\lambda \sin\theta_m FBW << 1$, or to cases where tapped delay lines are used to synthesize broadband weights.

Finally, we have shown that the nulling resolution against single source scenarios can be decomposed into resolution in two orthogonal directions: one direction, $\bar{\rho} - \underline{\rho}_r$, contains the plane of the average element location and the reference element location. Resolution in this plane is only weakly dependent on array configuration and is strongly dependent on the location of the reference element. Resolution in the direction orthogonal to $\bar{\rho} - \underline{\rho}_r$ tends to be independent of the location of the reference element, and directly proportional to the HPBW of $E_m(u,v)$ for the given array configuration.

REFERENCES

1. S. P. Applebaum, "Adaptive Arrays", Technical Report SPL 66-1, Syracuse Universty Research Corp., (August 1966).

2. J. T. Mayhan "Nulling Limitations for a Multiple-Beam Antenna", IEEE Trans. Antennas Propag. AP-24 (November 1976).

3. M. L. Burrows and J. T. Mayhan, "Configuration Tradeoffs for Satellite Nulling Arrays", Technical Note 1978-5 Lincoln Laboratory MIT (21 November 1978) DDC AD-A065287.

4. A. Ishimaru, "Theory of Unequally Spaced Arrays", IEEE Trans. Antennas Propag. AP-10, (November 1962).

5. Y. L. Chow, "On Grating Plateaux of Nonuniformly Spaced Arrays", IEEE Trans. Antennas Propag. AP-13 (March 1965).

6. M. I. Skolnik, "Nonuniform Arrays", Antenna Theory: Part 1, Chapter 6, (McGraw Hill, New York, 1969).

7. J. T. Mayhan, "Some Techniques for Evaluating the Bandwidth Characteristics of Adaptive Nulling Systems", IEEE Trans. Antennas Propag. AP-27 (May 1979).

UNCLASSIFIED

SECURITY CLASSIFICATION OF THIS PAGE *(When Data Entered)*

REPORT DOCUMENTATION PAGE	READ INSTRUCTIONS BEFORE COMPLETING FORM
1. REPORT NUMBER: ESD-TR-80-27	2. GOVT ACCESSION NO.: AD-A088 592
3. RECIPIENT'S CATALOG NUMBER	
4. TITLE *(and Subtitle)*: Optimal Properties of the Circular Array for Use as an Adaptive Antenna	5. TYPE OF REPORT & PERIOD COVERED: Technical Note
	6. PERFORMING ORG. REPORT NUMBER: Technical Note 1980-3
7. AUTHOR(s): Joseph T. Mayhan	8. CONTRACT OR GRANT NUMBER(s): F19628-80-C-0002
9. PERFORMING ORGANIZATION NAME AND ADDRESS: Lincoln Laboratory, M.I.T. P.O. Box 73 Lexington, MA 02173	10. PROGRAM ELEMENT, PROJECT, TASK AREA & WORK UNIT NUMBERS: Program Element No. 33126K
11. CONTROLLING OFFICE NAME AND ADDRESS: Defense Communications Agency 8th Street and So. Courthouse Road Arlington, VA 22204	12. REPORT DATE: 17 April 1980 13. NUMBER OF PAGES: 42
14. MONITORING AGENCY NAME & ADDRESS *(if different from Controlling Office)*: Electronic Systems Division Hanscom AFB Bedford, MA 01731	15. SECURITY CLASS. *(of this report)*: Unclassified 15a. DECLASSIFICATION DOWNGRADING SCHEDULE

16. DISTRIBUTION STATEMENT *(of this Report)*

Approved for public release; distribution unlimited.

17. DISTRIBUTION STATEMENT *(of the abstract entered in Block 20, if different from Report)*

18. SUPPLEMENTARY NOTES

None

19. KEY WORDS *(Continue on reverse side if necessary and identify by block number)*

nulling resolution
antenna field of view
adaptive antenna
thinned array configurations

20. ABSTRACT *(Continue on reverse side if necessary and identify by block number)*

In order to achieve good resolution with few elements, highly thinned arrays used in conjunction with adaptive antenna pattern control are commonly employed. This paper develops thinned array configurations optimized in performance in accordance with specific criteria. These criteria are used to optimize the element positions within the array considering both the close-in nulling resolution, and the average coverage area over a fixed, circular field of view for which it is desired that system users have positive link margin to a satellite at geosynchronous altitude. It is determined that the circular array configuration, with elements equi-spaced on the circle, generally produces the best close-in nulling resolution against arbitrary interference scenarios for large values of D/λ.

DD FORM 1 JAN 73 1473 EDITION OF 1 NOV 65 IS OBSOLETE

UNCLASSIFIED

SECURITY CLASSIFICATION OF THIS PAGE *(When Data Entered)*